On the diversity of accommodation mechanisms in the tribology of Bulk Metallic Glasses

Pierre-Henri Cornuault [1*], Guillaume Colas [1], Alexis Lenain [2], Rémi Daudin [3], Sébastien Gravier [2]

[1] Femto-ST Institute – DMA Department, UBFC, CNRS UMR 6174, Besançon, France
[2] Vulkam Inc. Amorphous metal micro casting / www.vulkam.com / France
[3] University of Grenoble Alpes, CNRS, SIMaP, 38000, Grenoble, France

* corresponding author: pierre-henri.cornuault@ens2m.fr
+ 33(0)381402854

Abstract
Bulk Metallic Glasses (BMG) have exceptional mechanical properties compared to their traditional crystalline counterparts. However, BMGs often exhibit scattered tribological behaviours. To better understand the underlying mechanisms governing the behaviour of BMGs, four different alloys ($Zr_{52.5}Ti_5Cu_{17.9}Ni_{14.6}Al_{10}$, $Cu_{47}Zr_{46}Al_7$, $Cu_{60}Zr_{33}Ti_7$, and $Ni_{62}Nb_{33}Zr_5$) were studied in pure sliding, reciprocating conditions. The study shows that the residual elements coming either from the counterpart or the surrounding environment plays a major role in their tribological behaviour. The composition of the BMG have a lower impact in the process. Eventually, the study concludes that optimization of the tribological behaviour of the BMGs might not necessarily rely on optimizing BMG composition but might rather rely on optimizing the choice of counterparts as a function of contact conditions.

Keywords: metallic glass, tribology, tribochemistry

1 Introduction

Bulk Metallic Glasses (BMG), also known as amorphous metal alloys (AMA) have exceptional mechanical properties compared to their traditional crystalline counterparts: yield strength close to theoretical limit, high hardness, high elastic deformation capacity, high fatigue strength [1]. For a long time limited by manufacturing processes inducing geometries not very inclined to industrialization, parts in AMA can now be obtained industrially via an innovative process comprising two successive steps: (i) melting of a set of pure metal ingots defining the composition of the ultimate material, (ii) then extremely fast cooling of the liquid mixture in a mould resulting in solidification without crystal formation. The process then makes it possible to produce centimetre-sized parts with very high sub-micrometric geometric details and shape factors, in the absence of subsequent machining operations.

The novel properties of BMGs have naturally led to their interest in designing parts subjected to tribological contact, and consequently to friction and wear. This interest is now growing due to the need to miniaturize mechanical systems in many sectors, leading to more and more stringent sliding and rolling speeds and contact pressures. Tribological studies carried out over the last two decades have provided the following observations: (1) The wear resistance of BMGs is highly debated, with some authors finding that it is higher than that of crystalline alloys [2,3], others showing that it is lower or similar [4–7]. In addition, wear resistance significantly depends on the composition of the alloy and its mechanical properties, but in an unpredictable way. It is sometimes related to the hardness or the Young's modulus of BMG[1,8], and sometimes not [5,6]. (2) The friction coefficients measured on BMGs are generally very high (0.4 to 1) [2,4,9] and vary significantly from one grade to another [6]. (3) The tribological mechanisms observed also vary a lot according to the friction conditions (speed, pressure, geometry, kinematics...) [2,3,6]. Complex but rather common phenomena of material transfer [2,4,9,10], establishment of a 3rd body at the interface [8–11], modification of the mechanical properties of the BMG by frictional heating [9,11–13] or oxidation [7,10,13–17] have been mainly observed. Less common is the appearance of specific subsurface phenomena such as shear bands underneath the surface and acting as “internal interfaces” [17], the

dependency of crack propagations on the environment [8]. Interestingly, the behaviours encountered depend very much on the erratic intervention of crystallization phenomena induced by friction [2,12]. According to some studies [1,8], an optimal crystallization threshold would minimize wear.

Despite their interesting mechanical properties, BMGs therefore exhibit scattered tribological behaviours, often mediocre but sometimes excellent, and especially unpredictable or even often contradictory depending on the contact conditions [3]. Thus, a better understanding of the "composition / friction condition / tribological behaviour" coupling is necessary in order to make the tribological performance of BMGs more reliable.

The wide variety of the composition of BMG is a real strength as they might "easily" be tuned to fit the targeted tribological application. On the other hand, such a wide variety of compositions makes it hard to determine the mechanisms governing their tribological behaviour. The literature shows that the compositions of BMGs tested for applications that are of interest in this study, i.e. tribological application in which sliding occurs, are alloys mostly based (main element in weight%) is Cu, Zr, Ni, Fe, Ti [3,6,18]. The literature shows that Cu and Ni-based alloys showcase among the lowest volume loss on pin on disc test [6] while Ni and Zr-based alloys exhibit extended wear lives in gear applications [3,18]. Ni-based particularly demonstrated an extension of micro-gear wear life by a factor of 313 as compared to common SK-steel [3]. Consequently, 4 different alloys (2 Cu-based, 1 Zr-based and 1 Ni-based) are chosen for the study.

2 Experiment

2.1 Materials

For the present study, four different compositions of (BMGs) were processed: two Cu-based ($Cu_{47}Zr_{46}Al_7$ and $Cu_{60}Zr_{33}Ti_7$), one Zr-based ($Zr_{52.5}Ti_5Cu_{17.9}Ni_{14.6}Al_{10}$) and one Ni-based ($Ni_{62}Nb_{33}Zr_5$). Nevertheless, considering alloys composition, they will be named Zr, CuZr, Cu, and Ni throughout this paper for the sake of clarity. Table 1 gives the correspondence between the name and the actual composition of each BMG.

The primary alloys were produced by arc-melting (T>2500 °C) bulk fragments of the base elements of high purity (>99.9%) under argon atmosphere using a Ti getter for detection of any detrimental contamination traces. Each primary alloy was melted at least five times to ensure a high quality of the chemical homogeneity. The primary alloys were subsequently melted again and injected into dedicated moulds to produced plate-shaped samples (15 x 8 x 1 mm^3). The amorphous structure of each plate was confirmed by X-ray diffraction measurements using a Rigaku smartlab equipment with Cu-Kα radiation (cf. Supplementary Information (SI), Figure S 1).

The mechanical properties of each BMG are given in Table 1. Young's modulus and Poisson's ratio were measured using an ultrasonic echoes apparatus, Vickers hardness was measured with a load of 1 kg (10 measurements to ensure meaningful average and deviation calculation), and yield strength values were determined thanks to mechanical tests performed in compression. Cylinders with 2 mm in diameter and 4 mm in length were prepared for uniaxial compressions tests at room temperature. At least 3 tests were performed for each composition to ensure good reproducibility in results.

Sample denomination	Composition [at%]	Young's modulus [GPa]	Poisson's ratio	Yield strength [MPa]	Hardness [HV]
Zr	$Zr_{52.5}Ti_5Cu_{17.9}Ni_{14.6}Al_{10}$	91±2	0.36	1900±50	496±6
CuZr	$Cu_{47}Zr_{46}Al_7$	96±2	0.37	2070±60	512±9
Cu	$Cu_{60}Zr_{33}Ti_7$	96*	0.37	2160*	596±9
Ni	$Ni_{62}Nb_{33}Zr_5$	153±4	0.33	3060±120	798±8
Ball	100Cr6	210	0.29	750	805

Table 1 - Studied Bulk Metallic Glasses (BMGs) designation, composition, and mechanical properties. Asterix refer to data extracted from the literature [19], and mechanical properties of the ball are provided by the supplier.

2.2 Friction tests

Friction and wear properties of the 4 over-mentioned BMGs were tested in dry sliding condition against a 6 mm diameter 100Cr6 steel ball counterpart. Before experiments, both balls and plates were ultrasonically cleaned in absolute ethanol during 5 min and then dried in air. Ball-on-plate friction tests were performed at room temperature (22 ± 2 °C) and in ambient air using a tribometer achieving reciprocating linear motion with a ± 1 mm displacement stroke at 1 Hz. N_{cycles} = 10,000 backward-and-forward friction cycles were achieved, resulting in a 40 m total sliding distance with a 4 mm/s sliding speed. A constant normal force F_N were applied throughout the test using dead loads. The tribological behaviour of the 4 studied BMGs were compared by applying the same initial maximal hertzian contact pressure P according to (1).

$$(1) \quad P = \left[\frac{6\,F_N\,E^{*2}}{\pi^3\,R^2}\right]^{1/3}$$

where R = 3 mm is the ball radius, and E^* is the reduced Young's modulus of the contact defined with the Young's moduli and Poisson's ratios of the ball (E_1 = 210 GPa and ν_1 = 0.29) and of the tested BMG (E_2 and ν_2 defined in Table 1), such that:

$$(2) \quad E^* = \left[\frac{1-{\nu_1}^2}{E_1} + \frac{1-{\nu_2}^2}{E_2}\right]^{-1}$$

Two test configurations were performed depending on the initial contact pressure applied: low-pressure tests with P = 310 MPa, and high-pressure tests with P = 680 MPa. Consequently, depending on BMGs elastic properties (see Table 1), the constant normal loading applied during experiments ranged from 0.14 to 0.29 N for low-pressure tests, and from 1.52 to 2.98 N for high-pressure tests. Three friction tests per BMG samples and for each initial contact pressure were conducted to assess results reproducibility. Throughout each test, the relative displacement of the ball h and the friction force F_T were measured thanks to LVDT and piezoelectric sensors, respectively. Both signals were recorded with a 512 Hz frequency sampling. Data post-treatment were performed with a custom-made software allowing for plotting the local friction coefficient F_T/F_N versus h for each friction cycle. Figure 1 displays a typical example of such a friction cycle plot. In Figure 1, each circle point corresponds to the local friction coefficient measured in a given location of the friction track (in backward and forward motion direction).

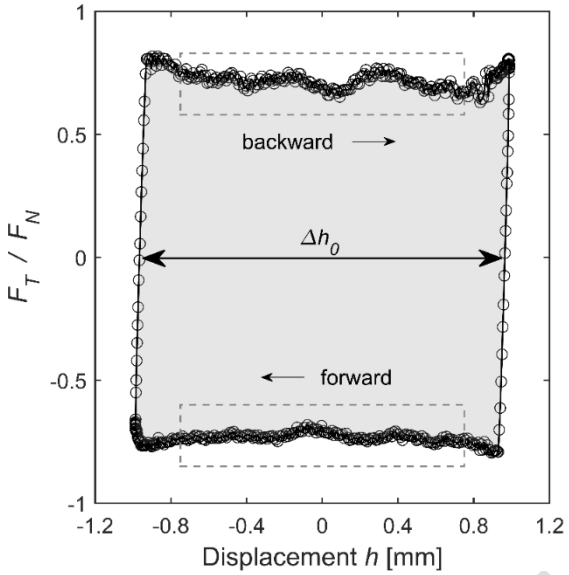

Figure 1 - Friction cycle F_T /F_N versus h typically obtained (here for Ni sample under 680 MPa hertzian maximal contact pressure and after 8,000 friction cycles previously performed).

Two quantitative descriptors of the contact frictional behaviour were then calculated from each friction cycles acquired. First, the friction coefficient μ related to the whole friction cycle was calculated from an energetic point of view using (3), where the integral refers to the grey filled area in Figure 1, and Δh_0 is the distance between the two positions on the friction track where $F_T = 0$ (very close to 2 mm).

$$(3)\quad \mu = \frac{1}{2\,\Delta h_0} \int \left|\frac{F_T}{F_N}\right| dh$$

Second, the variation of friction coefficient during a single back-and-forth motion $\Delta\mu$ was calculated as the standard deviation of the local F_T / F_N absolute values within the friction cycle. To exclude the instabilities owed to the reversal of the motion direction, only 75% of the measurements were taken into account, corresponding to the circle points positioned into the dashed grey line boxes in Figure 1.

2.3 Post-test analysis

After friction test, surface topography characterization of every friction tracks (balls and plates) were performed using a variable focus optical microscope (InfiniteFocus, Alicona Imaging GmbH). The three-dimension surface topography collected were then analysed with a specific home-made image treatment software in order to measure wear and friction track roughness. In this study, wear has to be intended as a lost volume of matter, meaning that phenomena such like material transfer can lead to negative wear values (matter addition). Figure 2 describes the advanced method that were followed for wear volume per unit of sliding distance calculation.

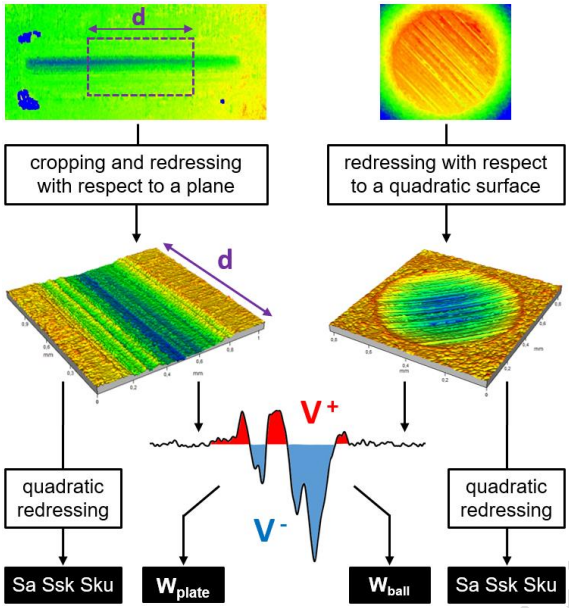

Figure 2 - Illustration of the method for Wplate, Wball, and friction tracks roughness parameters extraction. The scheme illustrating the determination of V + and V - is based on a profile analysis for the sake of clarity, but real volumetric measurements were performed

First, the plate friction track extremities were excluded by image cropping. Then, both plate and ball surfaces were flattened, subtracting the analytic closest plane and quadratic surfaces, respectively, which were obtained from the least-squares method. This step were performed by exclusion of the friction scar from the region of interest in both cases. Positive and negative volumes in reference to the average plane were then calculated for the plate (V_p^+ and V_p^-) and for the ball (V_b^+ and V_b^-). Finally, considering the sliding distance recovered by each parts, wear volumes per unit of sliding distance of the plate W_{plate}, of the ball W_{ball}, and of the overall contact W_{tot} (in µm^3/mm) were obtained using (4), where d is the track length in the analyzed cropped image (see Figure 2). This calculation has already been used in the literature [20] and provide a good base for comparisons.

$$(4)\quad W_{tot} = W_{plate} + W_{ball} = \frac{V_p^- - V_p^+}{2\,d\,N_{cycles}} + \frac{V_b^- - V_b^+}{4\,N_{cycles}}$$

The surface roughness parameters Sa (arithmetic mean height), Ssk (skewness), and Sku (kurtosis) were also calculated onto each friction track (balls and plates), after redressing it up according to the method mentioned above. Prior to tests, the mean and standard deviation of these parameters were measured from the analysis of ten balls and five 1×1 mm² original surface areas of each BMG plate, for comparison.

Friction tracks morphology and chemistry were also analyzed by Scanning Electron Microscopy (SEM) and Energy Dispersive Spectroscopy (EDS). SEM imaging were performed using a Zeiss ultra 55 MEG-FEG operated at 5 kV (Everhart-Thornley detector), and EDS analyses were conducted at 15 kV with a Bruker SD detector.

3 Results

3.1 Friction coefficient

Typical evolutions of the friction coefficient μ against sliding distance of the four tested BMGs are displayed in Figure 3(a) for low contact pressure tests (P = 310 MPa), and in Figure 3(b) for high contact pressure tests (P = 680 MPa). For the sake of clarity, a single curve representative of μ versus sliding distance is presented for each tested BMG in these figures. Nevertheless, very similar results were obtained when testing each sample in the same condition (cf. SI, Figure S 2). All plots show that μ tends to reach a steady-state value. The sliding distance needed for μ stabilization differs depending on the BMG and the pressure considered, but stabilization already occurred after approximately 25 m of sliding in any cases. The stabilized friction coefficient μ_{stab} were consequently defined and calculated as the mean value of μ between 30 and 40 m of sliding. The means of μ_{stab} and their standard deviation related to the three tests performed under the same contact pressure for each BMG are displayed in Figure 3(c).

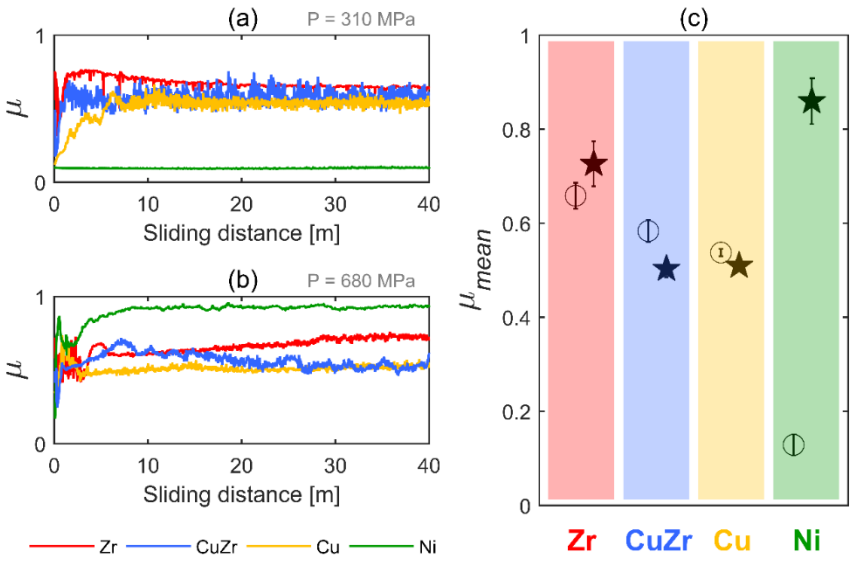

Figure 3 - Friction coefficient μ against sliding distance of the Zr (red), CuZr (blue), Cu (yellow), and Ni (green) samples for low contact pressure (P = 310 MPa) tests (a) and high contact pressure (P = 680 MPa) tests (b). Mean friction coefficient throughout the ten lasts meters of sliding μ_{stab} for the four BMGs (c). Unfilled circles and black stars refer to low and high contact pressure respectively, and bars are the standard deviations. (The reader is referred to the web version of this paper for the references to color interpretation).

Friction results reproducibility is attested by the relatively low value of μ_{stab} standard deviation (bar length) in all configurations. While differing at the very beginning of the tests, CuZr and Cu samples exhibit similar frictional behavior for the two contact pressures applied. μ_{stab} is approximately 0.55 under low contact pressure, and a very slight decrease of friction coefficient towards 0.5 is observed when the contact pressure increases. Zr sample exhibits higher μ_{stab} which increases only slightly from 0.66 to 0.73 with increasing contact pressure. Similar friction coefficients were reported in the literature for various Cu-based and Zr-based BMGs [21–24]. Conversely, Ni displays a very low and stable friction coefficient close to 0.1 throughout the test performed under 310 MPa. But μ_{stab} surprisingly reaches the very high value of approximately 0.9 under 680 MPa contact pressure. While few changes of friction coefficient related to the increase of pressure is observed for Zr, Cu and CuZr, it increases by a factor of 9 for Ni.

The variation of μ against sliding distance is commonly observed as an indicator of the tribo-contact interface stability. From this point of view, one can note in Figure 3(a) and (b) the better frictional stability of Ni as compared to the three other materials, regardless the pressure applied. But more relevant is to look at both the mean level and the variations of $\Delta\mu$ during the test. Indeed, while μ characterizes the whole mean level of friction integrating a complete back-and-forth motion cycle, $\Delta\mu$ reflects the local friction forces fluctuation along the track. Therefore, the evolution of $\Delta\mu$ versus sliding distance characterizes the local friction forces variation over time. Figure 4 shows $\Delta\mu$ evolution during the 5 lasts meters of sliding for the eight tests depicted in Figure 3(a) and (b).

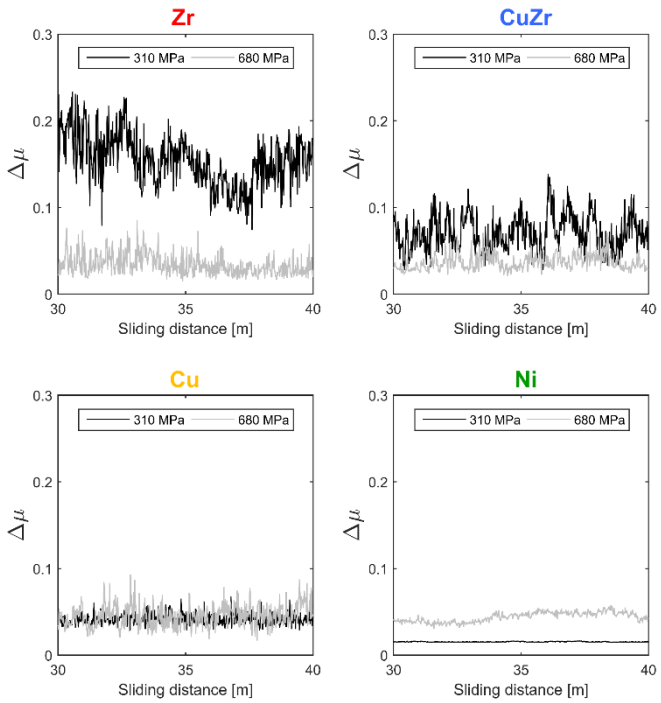

Figure 4 – Typical Evolution of the friction coefficient standard deviation Δμ during the ten lasts meters of sliding of the four tested BMGs, for low (black curves) and high (grey curves) contact pressure tests.

At P = 310 MPa, Figure 4 reveals a high level of fluctuation of the friction force at the Zr/steel ball interface along the friction track. Moreover, the level of fluctuations varies significantly from one friction cycle to another. These fluctuations are less pronounced in average for CuZr but still varied significantly over time. A tribometer effect [25,26] can be excluded because Zr and CuZr requires the highest normal loads to reach the defined contact pressure, while Cu and Ni require the lowest (down to the tribometer limit) and exhibit much lower fluctuations. Moreover, at high contact pressures, Zr and CuZr both exhibits the highest level of variations from one cycle to another. By contrast, the frictional behaviour of Ni/steel ball interface is very stable over time and throughout the friction track. At P = 680 MPa, the average level of friction force fluctuations is lower than for lower pressure tests, except for the Ni based BMG, but is similar between the four BMGs. Notwithstanding, the variations in the friction force fluctuations remains the lowest for the Ni. Note that even though Ni exhibits the highest coefficient of friction at P = 680 MPa, the friction coefficient is the most stable all over the steady state.

3.2 Wear volume

Figure 5 highlights the mean wear volumes per unit of sliding distance W_{plate}, W_{ball}, and W_{tot} calculated for the four studied BMGs. Under low contact pressure (P = 310 MPa), the overall wear of the contact is higher for Zr than for CuZr and Cu which display similar results. The wear of the Ni/steel ball tribo-system is very low: it decreases by approximately a factor of 10 and 6 as compared to Zr and Cu respectively. Considering Zr and CuZr contacts, the total wear is distributed between the BMG plate and the ball. Conversely, ball wear is negligible and the BMG plate bears the quasi-totality of the overall wear for Cu and Ni contacts.

As commonly expected, wear increases as the applied contact pressure increases. An increase of W_{tot} and W_{plate} by approximatly factor of 7 when P is doubled can be retained as an order of magnitude, regardless the BMG considered. The increase of W_{ball} with P is more complex and depends on the counterpart BMG nature. Under high contact pressure (P = 680 MPa), the classification of BMGs with regard to W_{tot} remains nearly the same than at low contact pressure, while Cu achieved significantly higher wear than CuZr. The ball's wear dominates for the Zr/steel ball tribo-sytem while the BMG plate is mainly worn for the three others contacts. Surprisingly, the overall wear of the Ni/steel ball tribo-system remains very low under high contact pressure despite its very high friction coefficient (μ_{stab} = 0.9). The wear of Ni is more than 5 times lower than that of Cu.

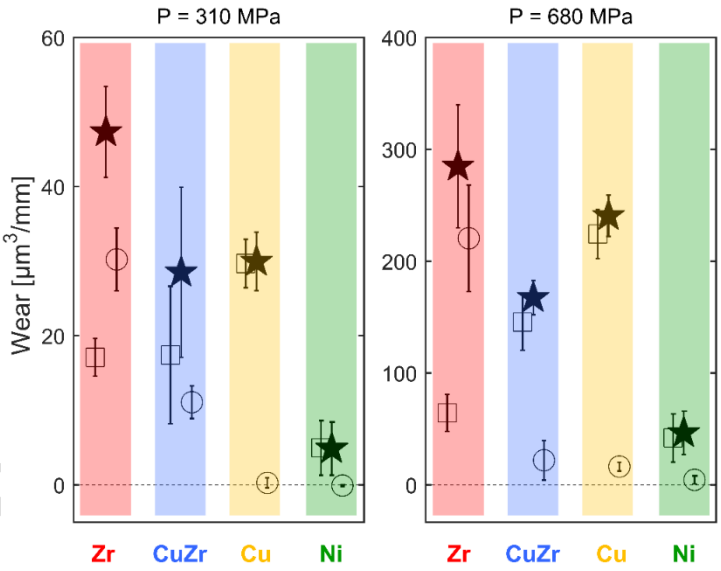

Figure 5 - Mean wear of the BMG plate Wplate (unfilled squares), mean wear of the steel ball counterpart associated Wball (unfilled circles), and mean wear of the whole contact Wtot (black-filled stars). Results are given for the four BMGs tested under low contact pressure (left) and high contact pressure (right). Bars are the standard deviations, and horizontal dotted lines refer to no-volume-change with respect to the original surfaces.

It should be noted that there is no correlation between wear and mechanical properties of the tested BMGs. The softer one (Zr) worn the ball while the hardest (Ni) did not. Moreover, Zr and CuZr are somewhat equivalent in terms of mechanical properties, and they exhibit opposite wear behaviour, the CuZr is indeed more worn than the ball. This is consistent with the literature which shows that wear resistance is not univocally a matter of hardness [1,5,6,8]

3.3 Surface roughness modification

Table 2 reports the means and standard deviations of the arithmetic mean height roughness parameter *Sa* which were calculated onto friction tracks (steel balls and BMG plates). Compared to the original unworn surfaces, *Sa* of BMG plates did not change a lot, except for Zr and CuZr after high contact pressure testing. More importantly, plate's surfaces have even been smoothed in many cases, especially for Cu and Ni BMGs. Nevertheless, ball's surface roughness significantly changes as compared to the original one. It becomes rougher and rougher when increasing the contact pressure for Zr, CuZr and Cu, especially for the Zr BMG counterpart. By contrast, the ball surface related to Ni counterpart gets smoother after low pressure tests and its roughness remains unchanged after high pressure tests.

	Zr	CuZr	Cu	Ni	
Sa of the Plate [µm]	0.73 ± 0.19	0.71 ± 0.09	0.60 ± 0.14	0.53 ± 0.13	Initial state
	0.41 ± 0.06	0.77 ± 0.15	0.49 ± 0.12	0.34 ± 0.13	P = 310 MPa
	1.25 ± 0.08	0.99 ± 0.26	0.44 ± 0.08	0.38 ± 0.11	P = 680 MPa
Sa of the Ball [µm]	0.54 ± 0.16				Initial state
	2.91 ± 0.19	2.26 ± 0.17	0.77 ± 0.23	0.22 ± 0.02	P = 310 MPa
	7.75 ± 0.72	3.00 ± 0.66	2.41 ± 0.28	0.54 ± 0.10	P = 680 MPa

Table 2 - Surface roughness parameters Sa mean values (black written) and their standard deviation (grey written) measured onto the friction tracks of the ball and the plate after friction tests performed with Zr, CuZr, Cu, and Ni-based BMGs under low (310 MPa) and high (680 MPa) contact pressure. Initial state refers to measurements performed before friction tests, on original surfaces.

Figure 6 displays the mean *Sa* values of each worn surface related to their wear volume (W_{plate} or W_{ball}). This graph highlights that balls surface modification is highly correlated with their wear volume, whereas BMG plate's wear processes do not lead to large surface roughness modification. These results suggest that BMGs are subjected to relatively smooth wear mechanisms. The smoothest surfaces (on both the plate and the ball) are obtained for Ni (at both 310 MPa and 680 MPa contact pressures) and then for Cu at 310 MPa contact pressure, that could explain why the friction coefficient fluctuations are among the lowest (Figure 4).

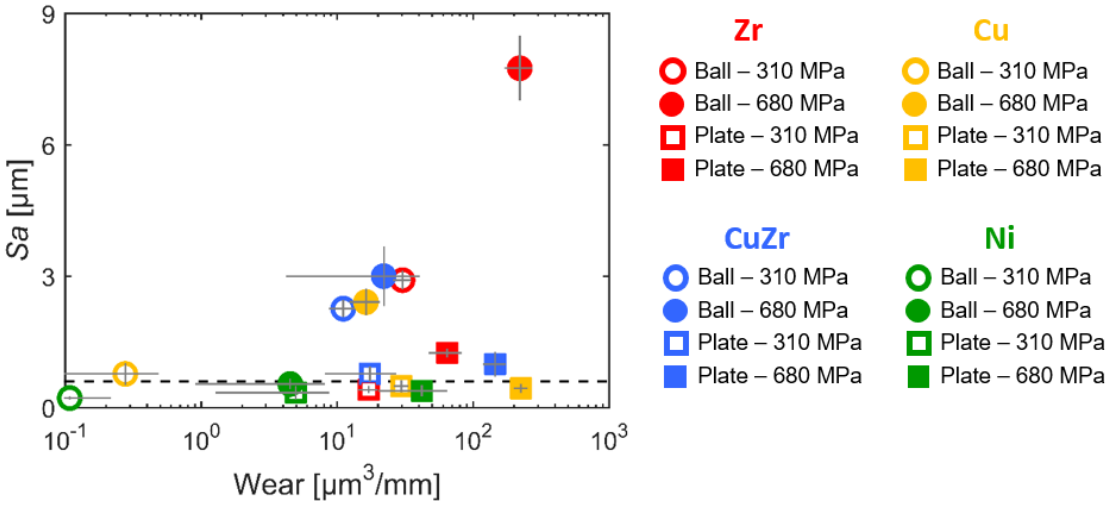

Figure 6 - Surface roughness parameters Sa mean values versus Wplate (squares) and Wball (circles) for the Zr (red), CuZr (blue), Cu (yellow), and Ni (green) tribo-systems. Data are given for low contact pressure tests (unfilled markers) and high contact pressure tests (filled markers). Standard deviations appear as gray bars. The horizontal dotted line corresponds to the mean Sa of unworn original surfaces.

In addition, it must be mentioned that few variations of *Ssk* and *Sku* were observed from the original surfaces to the worn ones in every test conditions for CuZr, Cu and Ni contacts (balls and plates). As *Ssk* remains close to 0 and *Sku* close to 3.5, surface's peaks height distribution can be considered as a Gaussian (*Ssk* = 0 and *Sku* = 3) slightly skewed above the mean plane. Notwithstanding, *Sku* measured on the Zr plate and the associated balls reaches 6.1 after both high and low pressure tests, meaning more peaks above the mean plane of the surface. This observation explain the fact that the low friction stability and high friction coefficient fluctuations all along the steady state is the highest as compared to the other BMGs tested (Figure 4). Such an important increase of *Sku* parameter has been observed by Rahaman et al [11], they attributed it to adhered debris distributed inside the friction track. To better understand the mechanisms leading to high *Sku*, there is a need to look closely at the surface morphology.

3.4 Flash-temperature estimation

Special emphasis has been placed in the literature concerning the effect of frictional heating on the tribological behavior of BMGs.[9,11] Indeed, the contacting temperature can eventually exceed the glass-transition and crystallization temperature of BMGs under some contact conditions (pressure, velocity…). Such transient and local temperature increase is commonly referred to flash-temperature.[27] In this case, viscous flow of the BMG partially occurs and significantly affects the friction and wear behaviors.[9] As pointed out by Kalin[28], numerous flash-temperature models were developed in the last thirty years to estimate interfacial heating which is besides difficult to measure experimentally. Although different, they are all commonly based on the Jaeger moving heat source model.[29] Notwithstanding, models frequently suffer from the necessary but difficult quantification of contact spots number and/or size. The maximal flash-temperature reached in the herein study was estimated through five different models originating from the works of Ashby-Abulawi-Kong[30,31] (used by Kong *et al*[9] for Cu-based and Zr-based BMGs sliding against Si_3N_4), Rahaman-Zhang[11] (used for a Ti-based BMG), Tian-Kennedy[32], Cook-Bhushan[33], and Greenwood.[34,35] Calculation was focused on the Ni-based BMG under high contact pressure since it corresponds to the highest flash-temperature due to high friction coefficient and low contact area achieved among all contact conditions tested. Flash-temperatures were computed for contact spots size ranging from 0.1 to 10 µm as realistic values, to account for the undetermined mean contact radius of the asperities. Within this range, all models give temperatures ranging from 300 to 343 K that are close to room temperature and very far from glass-transition and crystallization temperatures (cf. SI, Figure S 3). Results suggest the absence of severe interfacial heating which may result in material flow. They are consistent with low Péclet's number owed to low sliding speed and low normal load achieved in the herein experiments. The reader is referred to the Supplementary Information (SI) joined to this paper for further details on the flash-temperature expressions associated to each model and the set of parameters and numerical values used for calculation (see Table S 1 of the SI).

3.5 Friction tracks morphology and chemistry

To better define and understand what mechanisms are governing the tribological behaviours of the BMGs studied, friction tracks morphologies and elemental compositions on both the balls and the plates where analyzed using SEM and EDX instruments. For the sake of clarity and easy comparisons, morphologies and composition descriptions of the interfacial materials for every rubbed surfaces in both testing conditions have been summarized in Table 3. Figures are added when necessary to illustrate specific morphologies and compositions. Note that in all cases, ejected particles are isolated particles that are able to move freely. Those remaining at the extremities of the friction tracks are essentially iron oxide.

	Plate		Ball	
	Morphology	Composition	Morphology	Composition
Zr *(310 MPa)*	Regularly distributed thick 3rd body patches exhibiting ***periodic features*** (150 nm period)	Fe+O	Isolated thin 3rd body patches exhibiting ***periodic features*** (150 nm period)	Fe+O+(Cr)+(Si)
	Isolated particles distributed around and under the patches	Fe+O	Almost no isolated particle inside the contact	Fe+O
Zr *(680 MPa)*	Thick 3rd body patches all over the center of the track	Fe+O+(C)	No 3rd body patches Extremely thin tribofilm	-
	Isolated particles distributed around and under the patches	Fe+O	Almost no isolated particle inside the contact	Fe+O+C
CuZr *(310 MPa)*	Few thick and large 3rd body patches, mostly on the edges of the track	Cu+Zr+O+(Al)	Few thick and large 3rd body patches	O+Zr+Cu+Fe+(Al)
	Thin dark spots homogeneously distributed all over the track,	C+Zr+Cu+O +(Al)	No dark spots	-
	Few isolated particles distributed around and under the patches	Cu+Zr+O+(Al)	Isolated particles mostly distributed around the patches	O+Fe+Zr+Cu +(Al)
CuZr *(680 MPa)*	Few thick 3rd body patches	O+C+Cu+Zr +(Al)	Few thick 3rd body patches	Fe+O+Zr+Cu+O+(Al)
	Thin dark spots covering the entire track	C+Cu+O+Zr +(Al)	No dark spots	-
	Few isolated particles distributed around and under the patches	Cu+Zr+O+(Al)	Layer of isolated particles covering the entire track	O+Zr+Cu+Fe+(Al)
Cu *(310 MPa)*	Isolated particle in the track	O+Cu+C+Zr+(Ti)	Isolated particles everywhere	Cu+Zr+O
	-	-	Thick 3rd body patches all over the track, numerous "bi-color" gray/**dark patches**	Gray: O+C+Zr+Cu+C Dark: C+Cu+O+(Zr)
	Heavily plasticized surface	BMGs native composition	Few **thin dark spots** on top of the steel, all over the track	C+O+Cu
Cu *(680 MPa)*	Isolated particle in the track	Zr+Cu+O+(Ti)	Few isolated particles	Cu+Zr+O+(Ti)
	-	-	Thick layer of 3rd body	C+Zr+Cu+O+(Ti)
	Heavily plasticized surface	BMG comp.	-	-
Ni *(310 MPa)*	Almost no isolated particle	Ni+O+C+Nb	Nothing detectable, looks like a polished steel surface	-
	3rd body layer of 3 morphologies: -Thick and compact -Thin agglomerate of small particles -Thin and compact	O+Ni+Nb+C Ni+O+C+Nb Ni+C+Nb+O		
Ni *(680 MPa)*	Thick 3rd body layer exhibiting ***periodic features*** (570 nm period)	Cr+O+(C)	Thick 3rd body layer exhibiting ***periodic features*** (570 nm period)	Cr+O+Ni+Nb
	No isolated particles at the edges of the track	-	Few isolated particles around the 3rd body patches	Cr+O+Ni+Nb

Table 3 - Morphologies and composition of the interfacial materials in the friction tracks on both the plate and the ball, for all tested materials under both low and high contact pressure. In the composition, the elements are displayed in the order of importance, i.e. the first the most detected. The element appearing in brackets are detected at less than 5% on atomic percentage.

From Table 3, the Zr is essentially degrading the ball with the creation of an interfacial material essentially comprised of iron oxide (at both 310 MPa and 680 MPa contact pressures). This appears quite surprising because the Zr is softer than the ball and one would expect the ball to be the least damaged. The morphologies of the friction tracks on the BMG plate and the ball suggests different wear modes. Long and large scratches are observed on the Zr plate, suggesting abrasion, while the surface of the ball appears more homogeneously marked suggesting a more adhesive wear. This is in good correlation with Blau [36] who tested the same alloy sliding continuously against 100Cr6 steel ball. The presence of almost exclusively iron oxide in the friction track can be related to the ability of the Zr alloy to detach and transfer small particles from the counterface as it has been observed by Wu et al [13] who showed detachment of hard cubic ZrO_2 from Yttria stabilized zirconia counterface. Another reason for the high detection of iron oxide could be a more thermodynamically favored oxidation reaction to create Fe_2O_3 and Fe_3O_4 oxides as compared to ZrO_2 or Cu_2O, however, from the enthalpy of formation (cf. SI, Table S 2) it is hard to conclude. Removal of iron oxide from the ball via adhesive wear appears the most relevant. Then, most of iron oxide particles are shown to be harder than the Zr alloy (cf. SI and Table 1) and thus can abrade it, which explains the abrasive wear behaviour of the Zr. Very interesting features appearing when looking closely at the surface. The Zr sees the creation of a layer of particles with the top surface of that very layer compacted into a thin continuous third body layer (giving the appearance of thick patch) on which the ball is sliding (Figure 8 and Figure 7). That is comparable to the glaze layer formed on top of oxide particles and creating hard but brittle patches that are carrying the load [37]. The layer of particles presumably allows for accommodating part of the shear stress thanks to higher degrees of freedom while the ball is sliding over the patch sitting on top of the particles. Consequently, the wear of the ball is more severe as compared to the Zr alloy because it is most likely governed by the kinetic of formation/ejection of those patches inside/outside the contact. The fact that the Zr alloy is softer than the ball and the iron oxide particles, particles can "anchor" themselves on its surface and allow the build up of the patch. That can explain why the ball is not exhibiting the presence of patches. This is in good correlation with the wear volumes (Figure 5) and this most likely explaining why the friction coefficient exhibits similar values in both cases (Figure 3). Note that the significant presence of thick 3rd body patches and iron oxide particles inside the friction track on the plate of Zr at both low and high contact pressure is the reason for the high Sku measured on the Zr plates. Finally, Zr (310 MPa) is exhibiting periodic features on the 3rd body patches on both the ball and the plate (Figure 9). Such an observation ask the question of instabilities and/or stick slip modes inside the contact. That could explain the very high level of fluctuations of the friction forces exhibited by Zr at low contact pressure as compared to high contact pressure, considering that accommodation modes are otherwise similar in both cases (mainly rolling of iron oxide particles).

Conversely, the other 3 BMGs are essentially degrading themselves to create the interfacial material that is trapped inside the contact to accommodate the relative velocities between the ball and the plate. That is again in good correlation with wear volumes (Figure 5). Although they all behave differently, they exhibit the same types of 3rd bodies (Figure 7): isolated particles coupled with 3rd body patches (thick or thin) distributed all over the friction tracks. The CuZr acts as a transition material between those two extreme behaviours. On the ball, iron is mixed with the CuZr constitutive elements, reminding the presence of iron oxide in the 3rd body observed in Zr friction tracks. Interestingly, there is no trace of Fe detected inside the friction track on the CuZr plate, C and O are however highly detected. Previous studies [10,38] on the exact same material showed that the oxide layer on top of the metallic glass is mostly comprised of ZrO_2, then Cu_2O, and a very small portion of Al_2O_3, that is consistent with the EDS analysis of the friction track at low load. At high load, however, Cu and C are highly detected as compared to Zr. Louzguine-luzgin et al [38] also noticed that Zr was present in Zr^+ state and suspected that the reason might be a formation of ZrC compounds. If Zr is indeed reacting with carbonaceous elements, then O might react more with Cu potentially changing the proportion of elements. Based on the morphology of the friction tracks, the accommodation of relative velocities is believed to be done by mixing different modes: mainly interface shearing (sliding of the ball over the patches), rolling (isolated particles), and

shearing in the volume of the patches. Kang et al [10] showed that shear and ploughing were the main mechanisms contributing to friction in their case, but the shear contribution increased upon contamination time, i.e. if oxidation increased. That consequently goes hand in hand with the oxidation detected and described above and the absence of significant ploughing.

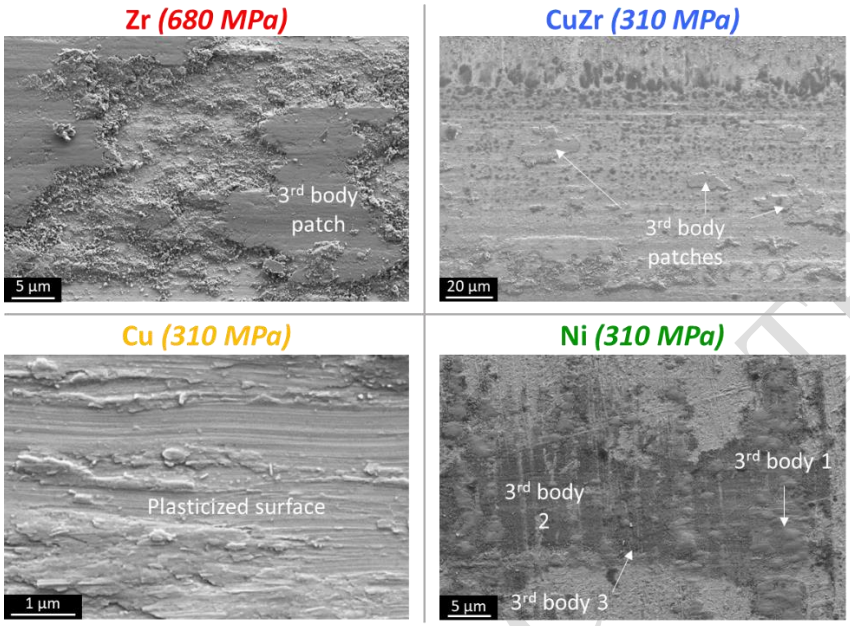

Figure 7 - SEM images of the main morphologies of 3rd bodies observed in the friction tracks of BMGs

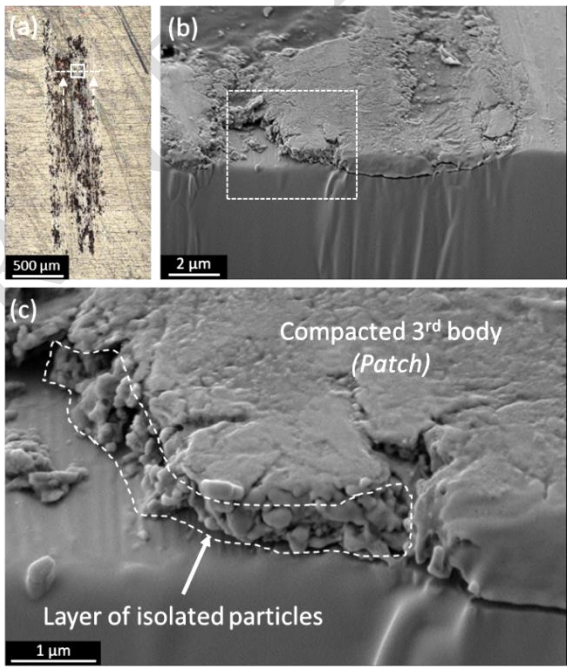

Figure 8 - SEM image of the 3rd body cut with the FIB, after tests with the Zr under high contact pressure. (a) optical image of the friction track with identification of the area where the FIB milling was done (small white square); (b) and (c) SEM image of the 3rd body after FIB milling, (c) is a magnification of (b).

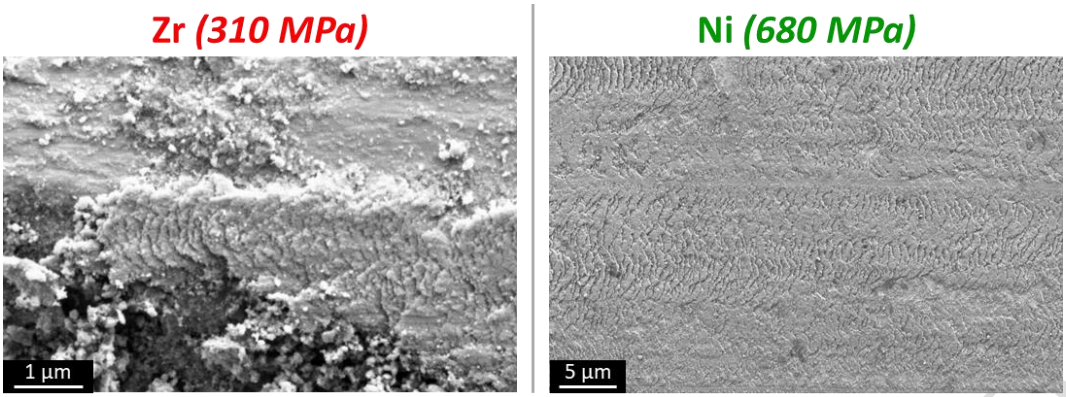

Figure 9 - Periodic features observed on the 3rd body created from the Zr and Ni

Interestingly, although CuZr and Cu have similar mechanical properties, their wear behaviour are very different (Figure 5), particularly at low load. Nonetheless, from Table 3 it can be assumed that similar oxidation behavior is taking place with Cu. Cu and CuZr are exhibiting similar composition of the materials created inside the tracks while their native composition is very different. For both BMGs, the Cu/Zr ratio is many times close to 1 and sometimes in favor Zr (Figure 10) although in the initial composition of Cu, the ratio is in favor of Cu. Zr diffusion to the native oxide layer formed at the surface of the bulk has been showed to happen naturally combined with Cu diffusion towards the interface between the oxide layer and the pristine bulk material [38]. That may have been enhanced by friction stress and induced temperature. C is again demonstrated to play a major role in the composition of the interfacial materials. The Cu is indeed exhibiting the presence of dark spots, numerous in the case of CuZr it is rather scattered and mixed with the 3rd body patches material for Cu (Figure 7 and Figure 10). The addition elements, Al and Ti, appears to have a minor impact on the compositions as they are always detected at less than 5% in atomic percentage of the composition of those features. Significant transfer of the element from Cu alloy to the ball is detected, which is consistent with the high wear volume measured on the Cu plate (Figure 5). Transfer appears to be done via adhesive wear. The friction track morphology shows that ploughing and shear appear to be highly contributing to friction (Figure 7). That is consistent with the fact that the deformation and fracture of this alloy is controlled by localized shear deformation [19]. Similarities in Cu and CuZr friction coefficients, in mechanisms contributing to friction, and in the composition of friction tracks most likely suggest that in steady state interface shearing is contributing more to friction as compared to ploughing. Differences in wear would thus be the consequence of the different kinematics involved to reach the steady state.

	A%(C)	A%(O)	A%(Ni)	A%(Zr)	A%(Nb)
3rd body 1	7.1	47.7	29.4	2.2	13.6
3rd body 2	21.0	25.3	34.7	2.5	16.5
3rd body 3	22.1	10.0	47.2	2.9	17.8

Table 4 - Quantitative analysis of the 3rd bodies seen on the friction track of the Ni based BMG after sliding at low contact pressure

The Ni stands out of the others. First, Zr is never detected although it is part of the composition of the Ni based BMG. Secondly, the material exhibit very different tracks compositions at low contact pressure and at high contact pressure. At low contact pressures (310 MPa), only O, Ni, Nb, and C are detected with different ratios depending on the type of 3rd body (particle, thin or thick patch). The quantitative analysis (Table 4) from the EDS measurements on the 3 types of 3rd bodies (cf. Figure 7) shows that Nb_2O_5, NiO and NbC are most likely present in the track. Nb_2O_5 appears to be the most plausible species comprising 3rd body 1 due to its highly negative formation enthalpy (cf. Table S 2 in SI). No traces of Fe is detected, which makes sense as the ball appears only polished without identifiable damage. The accommodation of sliding velocities appears to be handled by the 3rd body 1 that demonstrates compact

morphology and sliding features on top of it. That somewhat makes sense because the Nb_2O_5 oxide is soft compared to the BMG and the ball (cf. SI, Table S 2 for hardness values) and would thus flow more easily inside the contact to accommodate velocities. That means interface shearing appears to be the main mechanisms contributing to friction. At high contact pressures (680 MPa), even if some Zr is constituting 5% of the BMG, it is never detected in the composition of the interfacial material, the Cr initially contained within the 100Cr6 ball with a percentage within the range of 1.35 to 1.6% is significantly detected. The 3rd body composition is essentially made of Cr and O in the tracks on the BMG, as shown on the EDX map displayed on Figure 11. On the ball, it is a mix of Cr, O, Ni, and Nb. This observation combined with the evidence of very smooth surfaces on both the plate and the ball demonstrate a gentle process of transfer of Cr to the plate and of Ni and Nb to the ball. That means friction triggers the Cr diffusion in the steel from the bulk to the surface and its reaction with O coming from the atmosphere, and the Ni and Nb coming form the BMG. Once in the contact, the formation of Cr_2O_3 can happen very quickly (formation enthalpy highly negative (cf. SI, Table S 2)) and can help to protect the contact from further damage thanks to its high hardness (cf. SI). Such tribologically activated diffusion has been observed in other studies with the diffusion of Si from the bulk to the surface of an AISI440C ball (Si contained at less than 1% in it) [39]. Surprisingly, Ni is highly detected in the friction track while it has been shown that the native oxide layer on top of a $Ni_{62}Nb_{38}$ metallic glass is essentially composed of Nb_2O_5 oxide with Ni concentrated at the interface between the oxide layer and the bulk [14,15]. A synergistic mechanical – physicochemical phenomena appears to drive those changes. Interface shearing also occurs but mostly for the Ni at high load. There is almost no wear, no traces of isolated particles, but only a thick 3rd body layer. Similarly to Zr (310 MPa), the 3rd body exhibits periodic features (Figure 9) which could be related to instabilities and/or stick slip modes inside the contact. That may explain the increase of standard deviation of friction coefficient compared to the low contact pressure case (Figure 4). Higher adhesion would also explain the much higher friction coefficient observed at high load (Figure 3). As suggested by Wu et al [40], it is believed that adhesion is contributing to the creation of those patterns.

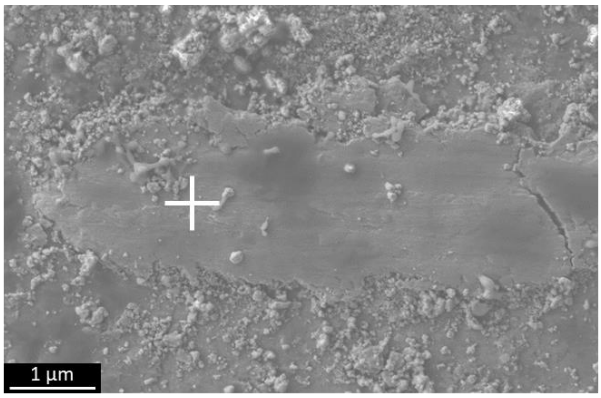

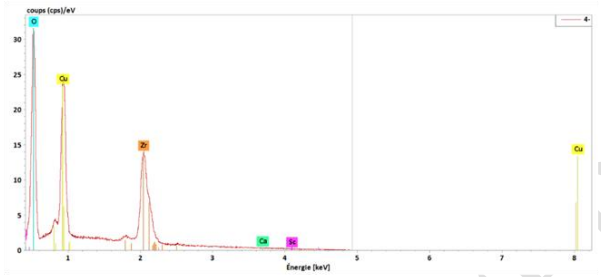

Element	C	O	Cu	Zr
Atomic [%]	17.05	46,37	15,34	20,91

Figure 10 - EDX spectra of the 3rd body patch created from the CuZr during low contact pressure friction tests. The analysis is conducted on the ball, the table present the atomic percentage of the main elements constituting the 3rd body.

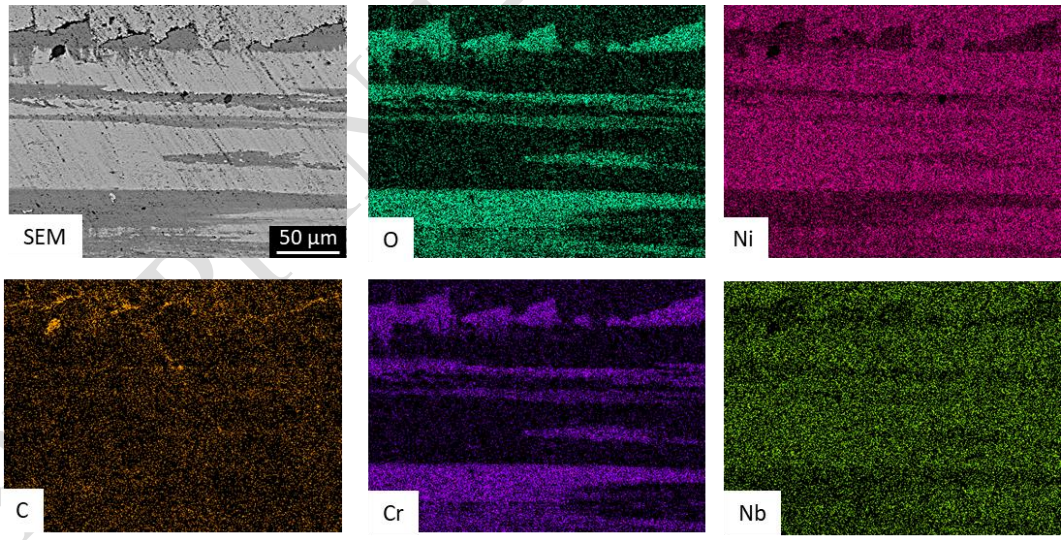

Figure 11 - EDX analysis of the friction track of the Ni sample after friction test at high contact pressure.

4 Discussion

The study shows that the lowest wear is obtained from Cu and Ni. This is in line with recent studies showing that Cu and Ni based alloys showcase among the lowest volume loss on pin on disc test [6]. The results presented here is also a good demonstration that high friction does not mean higher wear and that high friction is not necessarily implying noisy signal. Indeed, the Ni is exhibiting the highest friction of

all the tested materials when undergoing a friction tests at high contact pressures. However, it is also exhibiting very low wear for both the BMG plate and the steel ball. This is believed to be due to the selective tribochemistry occurring between the Cr (residual element from the ball) and the Ni and Nb from the BMG. Such a behaviour has already been seen in a previous study where a AISI440C/AISI440C contact demonstrated high friction (0.8 to 0.9 friction coefficient) and extremely low wear [39]. In that case reactions between water and the Si contained at less than 1% in the AISI440C were leading to the creation of a 3rd body protecting the surface from heavy damage.

Moreover, at high contact pressure, Zr and CuZr both exhibit the highest level of variations from one cycle to another. There are two possibilities to explain those behaviours: (i) they all have interfacial materials based (exclusively or partly) on iron oxides present inside the contact, and (ii) the Zr element plays a role in it by enhancing abrasion of the steel and consequently its oxidization. The first option is relevant to the high friction coefficient and high wear (the highest of all tests) that are observed. The second option is hardly conceivable because it would contradict the fact that the Cu is not exhibiting high variations in the friction coefficient fluctuations, especially as it has been shown that in the 3rd body zirconium sometimes dominates copper in proportion. That change in the elements proportion in the compositions of the 3rd bodies is once again an example of the selective tribochemistry happening inside the contact and observed in other tribological contacts [39,41,42]. Besides this interesting change in proportions of elements, the Cu is showing an interesting tribochemical process involving C. C and O are demonstrated to play a major role in the composition of the interfacial materials, inducing high sensitivity/reactivity of the Cu studied here towards carbonaceous species, O_2 and/or H_2O. There is indeed a significant creation of a 3rd body/tribofilm essentially comprised of carbon and distributed all over the friction tracks. As the dark spots are only located inside the tracks, the authors are confident this is not carbonaceous contamination issue but the real composition of the tracks. The literature shows that it is possible to tribologically trigger reactions with carbonaceous molecules coming from the air and leading to the creation of a lubricating material [20,43,44]. Furthermore, Louzguine-luzgin [38] suspected that the creation of ZrC compounds was also possible via reactions with carbonaceous species.

The tribochemical phenomena occurring inside the contact during friction tests of both Ni and Cu materials can be compared to the tribochemical competitions observed in several studies and in which, depending on the balance of reactive molecules coming from the environments and the base element of the materials, multiphasic materials are created [44–46]. For example, in Ti-doped DLC lubricated by PAO oil with ZnDTP and MoDTC additives [45], the reduction of the friction coefficient appears to result from beneficial competitive adsorption of ZnDTP and MoDTC on the surfaces. In that case, a selective tribochemical process occurred and led to the creation of Ti-rich and Zn-rich regions. This could be related to the biphasic third body observed with the Cu based BMG and the reactivity with carbonaceous species. Such reactivity was also demonstrated to be beneficial in [44] where lubricious DLC materials was created under friction of nanocrystalline Pt/Au alloy against sapphire. In a study of superlubricity of a-C:H:Si films, Chen et al. [46] showed that a critical balance between partial pressure of gas molecules is required to allow the appropriate synergistic effect between phase transformation (e.g. sp^2 vs sp^3 formation), shear localization, and surface passivation. This can be compared to the creation of the Cr+O (presumably Cr_2O_3) phase protecting the Ni based BMG from wear, although the friction coefficient is very high here.

Finally, it has to be noticed that all phenomena identified and described in the study are happening at room temperatures, which demonstrate a strongly synergy between mechanics and physicochemistry that goes beyond classical tribochemistry phenomenon.

5 Conclusion

The study demonstrates that the tribological behaviour of the BMG is a complex balance between mechanical and physicochemical phenomena. It indeed showed that none obvious relationship between friction coefficients, wear, and track morphologies can be drawn.

In this study, four different Bulk Metallic Glasses (BMG) have been studied in pure sliding and reciprocating contact conditions, under two different initial contact pressures. To our knowledge, this is also the 1st in depth and detailed tribological study (including surface, composition, and material characterization) of BMG sliding against conventional 100Cr6 steel alloy that is widely used in industry. The study demonstrated several important fact:

- In the case of the Zr-based alloy ($Zr_{52.5}Ti_5Cu_{17.9}Ni_{14.6}Al_{10}$), the velocity accommodation and wear are essentially undertaken by the 100Cr6 ball via iron oxide formation and compaction inside the contact as commonly observed with crystalline metal alloy. This is a first evidence of the importance of the nature of the counterpart in the BMG tribological behaviour.
- In the case of the 3 other BMGs ($Cu_{47}Zr_{46}Al_7$, $Cu_{60}Zr_{33}Ti_7$, and $Ni_{62}Nb_{33}Zr_5$), the 3rd bodies' atypical composition highlight room temperature mechanics/phisicochemistry synergies inducing surprising and complex tribochemistry phenomena:
    - The deterministic role of residual elements coming either from the counterpart or the surrounding environment, and more particularly here the role of (i) C resulting from carbonaceous species adsorption or coming from the ball in which it is contained at less than 1%, and (ii) Cr coming from the ball in which it is contained at around 1.5% and that is essential to protecting the Ni-based BMG from wear at high contact pressure of 680 MPa.
    - BMGs can be self-sufficient in certain conditions to lubricate the contact, as shown with the Ni-based BMG that is lubricating the contact via oxides that naturally form at its surface.
    - BMGs with close composition can see the creation of similar third bodies via ratio readjustment of constituting elements, and this independently of the residual elements (case of the $Cu_{47}Zr_{46}Al_7$ and $Cu_{60}Zr_{33}Ti_7$ BMGs here).

Overall, the present study shows that the optimization of the tribological behaviour of BMGs might not necessarily rely on optimizing their composition but would rather rely on optimizing the choice of counterparts as a function of contact conditions (contact pressure and environment). As such, this study proposes a new approach consisting in finely tuning the counterpart chemistry for the optimization of tribological contacts that involve BMGs.

6 Acknowledgement

The authors wish to sincerely thank Mohita Chandiramani for spending time to perform most of the friction tests during her undergraduate internship, Luc Carpentier for his help in repairing the µtribometer, Betty Baudinot for machining dedicated sample holders in a very short time which allowed us to perform the tests in due time, Jean-Yves Rauch for helping us with the FIB, and Stani Carbillet for the complementary SEM images and EDX analysis.

7 References

1. Greer, A. L., Rutherford, K. L. & Hutchings, I. M. Wear resistance of amorphous alloys and related materials. *Int. Mater. Rev.* **47**, 87–112 (2002).
2. Fleury, E., Lee, S. M., Ahn, H. S., Kim, W. T. & Kim, D. H. Tribological properties of bulk metallic glasses. *Mater. Sci. Eng. A* **375**–**377**, 276–279 (2004).
3. Ishida, M. *et al.* Wear resistivity of super-precision microgear made of Ni-based metallic glass.

Mater. Sci. Eng. A **449**–**451**, 149–154 (2007).
4. Parlar, Z., Bakkal, M. & Shih, A. J. Sliding tribological characteristics of Zr-based bulk metallic glass. *Intermetallics* **16**, 34–41 (2008).
5. Prakash, B. Abrasive wear behaviour of Fe , Co and Ni based metallic glasses. *Wear* **258**, 217–224 (2005).
6. Hofmann, B. D. C. *et al.* Optimizing Bulk Metallic Glasses for Robust , Highly Wear-Resistant Gears. *Adv. Eng. Mater.* **19**, 1600541 (2017).
7. Jin, H. W., Ayer, R. & Koo, J. Y. Reciprocating wear mechanisms in a Zr-based bulk metallic glass. *J. Mater. Res.* **22**, 264–273 (2007).
8. Fu, X., Kasai, T., Falk, M. L. & Rigney, D. A. Sliding behavior of metallic glass Part I . Experimental investigations. *Wear* **250**, 409–419 (2001).
9. Kong, J., Xiong, D., Li, J., Yuan, Q. & Tyagi, R. Effect of Flash Temperature on Tribological Properties of Bulk Metallic Glasses. *Tribol. Lett.* **35**, 151–158 (2009).
10. Kang, S. J. *et al.* Importance of surface oxide for the tribology of a Zr-based metallic glass. *Friction* **5**, 115–122 (2017).
11. Rahaman, M. L. & Zhang, L. On the estimation of interface temperature during contact sliding of bulk metallic glass. *Wear* **320**, 77–86 (2014).
12. Rahaman, M. L., Zhang, L. C. & Ruan, H. H. Understanding the friction and wear mechanisms of bulk metallic glass under contact sliding. *Wear* **304**, 43–48 (2013).
13. Wu, H., Baker, I., Liu, Y., Wu, X. & Munroe, P. R. Effects of environment on the sliding tribological behaviors of Zr-based bulk metallic glass. *Intermetallics* **25**, 115–125 (2012).
14. Caron, A. *et al.* Effect of surface oxidation on the nm-scale wear behavior of a metallic glass. *J. Appl. Phys.* **109**, (2011).
15. Caron, A. *et al.* Structure and nano-mechanical characteristics of surface oxide layers on a metallic glass. *Nanotechnology* **22**, (2011).
16. Louzguine-Luzgin, D. V. *et al.* Exceptionally high nanoscale wear resistance of a Cu47Zr45Al8 metallic glass with native and artificially grown oxide. *Intermetallics* **93**, 312–317 (2018).
17. Louzguine-Luzgin, D. V., Ketov, S. V., Trifonov, A. S. & Churymov, A. Y. Surface structure and properties of metallic glasses. *J. Alloys Compd.* **742**, 512–517 (2018).
18. Hofmann, D. C. *et al.* Castable Bulk Metallic Glass Strain Wave Gears : Towards Decreasing the Cost of High-Performance Robotics. *Sci. Rep.* **6**, 1–11 (2016).
19. Dai, C.-L., Deng, J.-W., Zhang, Z.-X. & Xu, J. Cu−Zr−Ti ternary bulk metallic glasses correlated with (L → Cu8Zr3 Cu10Zr7) univariant eutectic reaction. *J. Mater. Res.* **23**, 1249–1257 (2008).
20. Curry, J. F. *et al.* Achieving Ultralow Wear with Stable Nanocrystalline Metals. *Adv. Mater.* **30**, (2018).
21. Rahaman, M. L., Zhang, L., Liu, M. & Liu, W. Surface roughness effect on the friction and wear of bulk metallic glasses. *Wear* **332**–**333**, 1231–1237 (2015).
22. Hua, N. *et al.* Tribological behavior of a Ni-free Zr-based bulk metallic glass with potential for biomedical applications. *Mater. Sci. Eng. C* **66**, 268–277 (2016).
23. Jiang, F. *et al.* Tribological Studies of a Zr-Based Glass-Forming Alloy with Different States.pdf. *Adv. Eng. Mater.* **11**, 925–931 (2009).
24. Wang, Y. *et al.* Effect of sliding velocity on the transition of wear mechanism in (Zr,Cu)95Al5 bulk metallic glass. *Tribol. Int.* **101**, 141–151 (2016).
25. Kohen, I., Play, D. & Godet, M. Effect of machine rigidity or degrees of freedom on the load-carrying capacity of wear debris. *Wear* **61**, 381–384 (1980).
26. Cunnimgham, J. *A Tribometer Users Guide For Space Mechanism Applications - ESTL-TM-139*. (1994).
27. Blok, H. THE FLASH TEMPERATURE CONCEPT. *Wear* **6**, 483–494 (1963).
28. Kalin, M. Influence of flash temperatures on the tribological behaviour in low-speed sliding : a review. *Mater. Sci. Eng. A* **374**, 390–397 (2004).
29. Jaeger, J. C. Moving sources of heat and the temperature of sliding contacts. *Proc. R. Soc. New South Wales* **76**, 203–224 (1942).
30. Lim, S. C. & Ashby, M. F. Wear Mechanism Maps. *Acta Mater.* **35**, 1–24 (1987).
31. Ashby, M. F., Abulawi, J. & Kong, H. S. Temperature Maps for Frictional Heating in Dry Sliding. *Tribol. Trans.* **34**, 577–587 (1991).

32. Tian, X. & Kennedy, F. E. Maximum and Average Flash Temperatures in Sliding Contacts. *J. Tribol.* **116**, 167–174 (1994).
33. Cook, N. H. & Bhushan, B. Sliding Surface Interface Temperatures. *J. Lubr. Technol.* 59–64 (1973).
34. Greenwood, J. A. An interpolation formula for flash temperatures. *Wearar* **150**, 153–158 (1991).
35. Greenwood, J. A. Surface temperatures in a fretting contact. *Wear* **155**, 269–275 (1992).
36. Blau, P. J. Friction and wear of a Zr-based amorphous metal alloy under dry and lubricated conditions. *Wear* **250**, 431–434 (2001).
37. Stott, F. H. & Wood, G. C. The influence of oxides on the friction and wear of alloys. *Tribol. Int.* 211–218 (1978).
38. Louzguine-Luzgin, D. V. *et al.* Bulk metallic glassy surface native oxide: Its atomic structure, growth rate and electrical properties. *Acta Mater.* **97**, 282–290 (2015).
39. Colas, G., Saulot, A., Regis, E. & Berthier, Y. Investigation of crystalline and amorphous MoS2 based coatings: Towards developing new coatings for space applications. *Wear* **330**–**331**, 448–460 (2015).
40. Wu, H. *et al.* Tribological studies of a Zr-based bulk metallic glass. *Intermetallics* **35**, 25–32 (2013).
41. Colas, G., Saulot, A., Descartes, S., Michel, Y. & Berthier, Y. Double Transfer Experiments To Highlight Design Criterion for Future Self-Lubricating Materials. in *Conference proceedings of the 16th European Space Mechanisms & Tribology Symposium* (2015).
42. Colas, G., Saulot, A., Philippon, D., Berthier, Y. & Léonard, D. Tribochemical competition within a MoS2/Ti dry lubricated macroscale contact in ultrahigh vacuum: a Time of Flight Secondary Ion Mass Spectrometry investigation. *ACS Appl. Mater. Interfaces* **10**, 20106–20119 (2018).
43. Colas, G. *et al.* How far does contamination help dry lubrication efficiency? *Tribol. Int.* **65**, 177–189 (2013).
44. Argibay, N. *et al.* In situ tribochemical formation of self-lubricating diamond-like carbon films. *Carbon N. Y.* **138**, 61–68 (2018).
45. Numata, T. & Sasaki, S. Mechanism of metal doping effect on lubricity of DLC films. in *Transient Processes in Tribology, Volume 43: Proceedings of the 30th Leeds-Lyon Symposium on Tribiology (Tribology and Interface Engineering)* (ed. G. Dalmaz, A.A. Lubrecht, D. D. and M. P.) 45–49 (Elsevier Science, 2004). doi:10.1016/S0167-8922(03)80033-0
46. Chen, X., Kato, T. & Nosaka, M. Origin of superlubricity in a-C:H:Si films: A relation to film bonding structure and environmental molecular characteristic. *ACS Appl. Mater. Interfaces* **6**, 13389–13405 (2014).